Legon, A., Tew, D., Medcraft, C., Gougoula, E., Bittner, D., Mullaney, J., ... Walker, N. (2017). Molecular Geometries and Other Properties of H2OAgI and H3NAgI as Characterised by Rotational Spectroscopy and Ab Initio Calculations. *Journal of Chemical Physics*, *147*(23), 234308-1-8. https://doi.org/10.1063/1.5008744

Journal of Chemical Physics

Molecular Geometries and Other Properties of $H_2O\cdots AgI$ and $H_3N\cdots AgI$ as Characterised by Rotational Spectroscopy and Ab Initio Calculations

Chris Medcraft,[a] Eva Gougoula,[a] Dror M. Bittner,[b] John C. Mullaney,[a] Susana Blanco,[c] David P. Tew,[d] Nicholas R. Walker[a,*] and Anthony C. Legon[d,*]

[a] Chemistry-School of Natural and Environmental Sciences, Newcastle University, Bedson Building, Newcastle-upon-Tyne, NE1 7RU, UK

[b] Present address: Department of Chemistry and Biochemistry, Old Dominion University, 4541 Hampton Boulevard, Norfolk, VA 23529-0126, USA

[c] Present address: Departamento de Quimica Fisica y Quimica Inorganica, Facultad de Ciencas, Universidad de Valladolid, 47011-Valladolid, Spain

[d] School of Chemistry, University of Bristol, Cantock's Close, Bristol BS8 1TS, UK

Corresponding authors email addresses: Nick.Walker@newcastle.ac.uk, a.c.legon@bristol.ac.uk

KEYWORDS: rotational spectroscopy, nuclear quadrupole coupling, hyperfine structure

Abstract

The rotational spectra of $H_3N\cdots AgI$ and $H_2O\cdots AgI$ have been recorded between 6.5 and 18.5 GHz by chirped-pulse Fourier-Transform microwave spectroscopy. The complexes were generated through laser vaporisation of a solid target of silver or silver iodide in the presence of an argon gas pulse containing a low concentration of the Lewis base. The gaseous sample subsequently undergoes supersonic expansion which results in cooling of rotational and vibrational motions such that weakly-bound complexes can form within the expanding gas jet. Spectroscopic parameters have been determined for eight isotopologues of $H_3N\cdots AgI$ and six isotopologues of $H_2O\cdots AgI$. Rotational constants, B_0; centrifugal distortion constants, D_J, D_{JK} or Δ_J, Δ_{JK}; and the nuclear quadrupole coupling constants, χ_{aa}(I) and χ_{bb}(I)–χ_{cc}(I) are reported. $H_3N\cdots AgI$ is shown to adopt a geometry that has C_{3v} symmetry. The geometry of $H_2O\cdots AgI$ is C_s at equilibrium but with a low barrier to inversion such that the vibrational wavefunction for the $v = 0$ state has C_{2v} symmetry. Trends in the nuclear quadrupole coupling constant of the iodine nucleus, $\chi_{aa}(I)$, of L···AgI complexes are examined, where L is varied across the series (L= Ar, H_3N, H_2O, H_2S, H_3P or CO). The results of experiments are reported alongside those of *ab initio* calculations at the CCSD(T)(F12*)/AVXZ level (X=T,Q).

I Introduction

Microwave spectroscopy has recently been applied to explore the molecular structures of complexes in which a Lewis base is attached to either CuX, AgX or AuX (where X is a halogen atom) to form L···MX [1-11], where for example L = H_2O[1, 10], H_2S[3-5], NH_3[12], C_2H_2[6, 8, 11] or CO[13, 14]. The same technique has also been applied to study complexes that are similar in composition and structure but distinct in that L is not a typical Lewis base. For example, H_2···MX[15, 16], Ar···MX[17-19], Kr···MX[18, 20] and Xe···MX[21] have each been characterised. Significant structural changes were identified in each of H_2[15, 16], C_2H_2[6, 8, 11] and C_2H_4[6] on their attachment to a coinage metal atom. Both H_2O···MX and H_2S···MX adopt pyramidal geometries of C_s symmetry at equilibrium. H_2O···MX complexes were observed to undergo rapid inversion between two equivalent C_s geometries on the timescale of a molecular rotation such that the geometry of H_2O···MX is effectively C_{2v} (planar) in the $v = 0$ state [1, 3-5, 10, 22]. Rotational spectroscopy has proven to be a powerful tool for investigation of the structure and dynamics in such complexes. Previous works have made comparisons with hydrogen- and halogen-bonded complexes of similar geometrical structure.

Examination of the trend in the nuclear quadrupole coupling constant of chlorine, χ_{aa}(Cl), across the L···AgCl[4, 8, 10, 15, 20, 21] series revealed that the attachment of argon to AgCl[19] induces only a very small change in the quantity relative to the value of the parameter in diatomic AgCl. The described change varies with L in the order; CO > H_2S > H_3N > H_2O. A very similar trend was observed in the equivalent L···CuCl series[4, 6, 10, 12]. The variation in χ_{aa}(Cl) provides an indication of the extent of electron redistribution accompanying the formation of each of these complexes. Evidently, stabilisation of OC···MCl through back-donation of electrons from d orbitals of the metal onto π* orbitals of CO leads to a stronger interaction than that existing within Ar···MCl. The present work aims to determine rotational constants, centrifugal distortion constants and nuclear quadrupole coupling constants of the L···AgI complexes for which L=H_2O or H_3N and use these quantities to draw conclusions about the geometries, interaction strength and electric charge redistribution associated with the complexes. The results will be compared with those from recent studies of other L···AgI, to allow trends to be established across a wide range of L···AgI for the first time.

II Methods

A Experimental

Broadband microwave spectra were measured using a chirped-pulse Fourier-transform microwave (CP-FTMW) spectrometer fitted with a laser ablation source. Detailed descriptions of the spectrometer and laser ablation source are provided in Ref. 9 and Ref. 23. The method employed to generate H_3N···AgI is

identical to that used previously during a study of $H_2S\cdots AgI$ [3,5] A gas sample containing a low concentration of precursors is diluted in argon and prepared at a total pressure of 6 bar. The sample is prepared to contain ~1.5% CF_3I and ~4.0% NH_3. The mixed sample is introduced into the spectrometer via a pulsed nozzle where it passes over the surface of a silver rod from which material is ablated by the 2nd harmonic of an Nd:YAG laser pulse (λ=532 nm, pulse duration of 10 ns, pulse energy of 20 mJ). The rotational and vibrational motions of molecules are subsequently cooled through supersonic expansion of the gas sample. The target rod is continually translated and rotated to expose a fresh surface to each laser pulse and ensure shot-to-shot reproducibility of signal intensities. Pulses are introduced with a repetition rate of approximately 2 Hz. Observations of rotational transition intensities suggest that the rotational temperature of probed species is of the order of 2 K. The generation of $H_2O\cdots AgI$ was achieved while using a solid target rod composed of silver iodide combined with a bespoke sample holder containing water and placed immediately in front of the nozzle[24]. Attempts to generate $H_2O\cdots AgI$ through vaporisation of a silver rod in the presence of gaseous H_2O and CF_3I precursors were unsuccessful. Isotopically-enriched samples of $^{15}NH_3$ (Sigma-Aldrich, 98% ^{15}N), ND_3 (Sigma-Aldrich, 99% D), D_2O and $H_2{}^{18}O$ were used to generate and record the spectra of isotopologues as appropriate.

The sequence employed to record broadband microwave spectra involves (i) polarization of the sample by a microwave chirp that sweeps from 6.5 to 18.5 GHz within 1 μs and then (ii) recording of the free induction decay of the molecular emission over a period of 20 μs. The sequence of (i) and (ii) is repeated eight times following each gas sample introduction pulse. The free induction decay (FID) of the polarization is digitized at 25 GS/s using a digital oscilloscope after down-mixing against a 19 GHz local oscillator. Frequency-domain spectra are obtained through Fourier transformation of the time-domain data to give a full width at half maximum (FWHM) of 65 kHz. The spectra of $H_3N\cdots AgI$ and $H_2O\cdots AgI$ were averaged for 600k and 570k free induction decays (FIDs) respectively prior to being Fourier transformed.

B Ab initio calculations

Geometry optimisations and frequency calculations were performed using the MOLPRO[25] and TURBOMOLE [26] packages at the CCSD(T)(F12*)[27] level of theory. The latter is a coupled-cluster method that includes single and double excitations, explicit correlation[28], and a perturbative treatment of triple excitations[29]. Basis set combinations consisting of aug-cc-pVXZ (X = T, Q) on C, H and N and aug-cc-pVXZ-PP (X = T, Q) on Ag and I with relativistic effective core potentials MDF-28[30,31] were used and will be referred to as AVXZ (X = T, Q). For the density fitting approximation which was used to accelerate the CCSD(T)(F12*) calculation, the respective def2-QZVPP basis sets were employed for the MP2 and Fock[32]

terms. For the complementary auxiliary basis required for the F12 treatment[33], the def2-TZVPP MP2 density fitting basis sets[32] were used. Only valence electrons were included in the correlation treatment.

III Results

A Measurement of Transition Frequencies

1 *$H_3N\cdots AgI$*

As described in Section IIA, the generation of $H_3N\cdots AgI$ was achieved by using CF_3I and NH_3 diluted in argon carrier gas interacting with the plasma produced by ablating silver. Transitions of CF_3I molecules were observed with high intensity, as were those of AgI. Transitions of $CF_3I\cdots NH_3$[34] were also observed but more weakly. Spectra containing AgI are distinctive by virtue of the characteristic isotopic abundance ratio of the two isotopes of silver and the hyperfine splitting introduced by the iodine nucleus (I=5/2). This distinctiveness greatly assisted the initial assignments of the spectra of $H_3N\cdots AgI$ shown in Figure 1. Subsequent experiments employed synthetically-enriched isotopic samples to confirm that these complexes are the carriers of the observed spectra and allowed measurements of shifts in the frequencies of transitions following isotopic substitution(s).

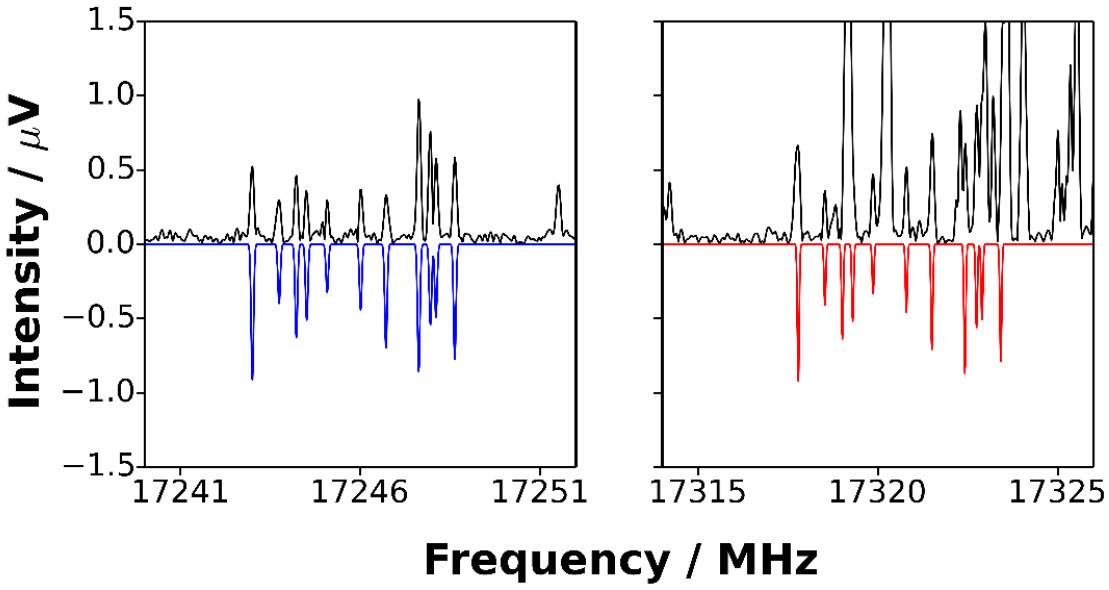

Figure 1. Expanded section of the spectrum recorded in the 6.5-18.5 GHz frequency range for $H_3N\cdots{}^{109}AgI$ (left) and $H_3N\cdots{}^{107}AgI$ (right) showing the $(J+1) \leftarrow J = 10 \leftarrow 9$ transition.). Blue and red downward pointing lines indicate the simulated spectra of isotopologues containing ^{109}Ag and ^{107}Ag respectively.

Spectra of the partially deuterated complexes, $H_2DN\cdots AgI$ and $HD_2N\cdots AgI$, were recorded in addition to that of $D_3N\cdots AgI$ during experiments that employed ND_3. It is assumed that H_2DN and HD_2N were each generated through reaction of a fraction of the introduced ND_3 sample with H_2O or NH_3 (perhaps present as a contaminant) within the sample vessel.

2. $H_2O\cdots AgI$

Laser vaporisation of silver iodide in the presence of argon and a low concentration of H_2O allowed the observation of intense features that assign to the AgI diatomic molecule[35]. Transitions of the Ar···AgI complex characterised previously[17] and a distinctive transition of the water dimer near 12321 MHz[36] were also observed. Series of other transitions share some qualitative features of the spectrum of Ar···AgI but were clearly associated with a different molecular carrier. The frequency increment between $(J+1) \leftarrow J$ transitions was consistent with a lighter molecule than Ar···AgI suggesting $H_2O\cdots AgI$ as a possible carrier (Figure 2). Subsequent experiments to probe $HDO\cdots AgI$ and $H_2{}^{18}O\cdots AgI$ isotopologues revealed isotopic shifts consistent with the assignment to $H_2O\cdots AgI$.

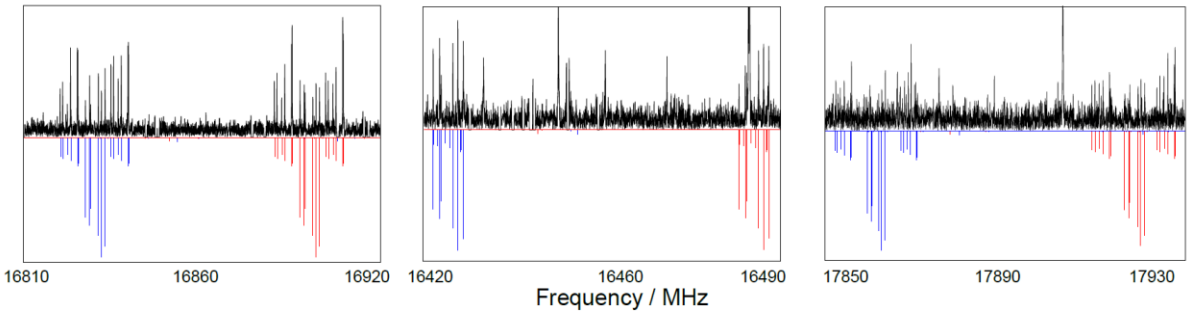

Figure 2. Expanded section of the spectrum obtained in the 6.5-18.5 GHz frequency range for $H_2O\cdots AgI$, $HDO\cdots AgI$ and $H_2{}^{18}O\cdots AgI$ (from left to right) in the regions of the $(J+1) \leftarrow J = 10 \leftarrow 9$ transition (first two panels) and the $(J+1) \leftarrow J = 11 \leftarrow 10$ transition (far right panel). Blue and red downward pointing lines indicate the simulated spectra of isotopologues containing ^{109}Ag and ^{107}Ag respectively.

B Spectroscopic Analysis

Parameters of the Hamiltonian shown in eq.(1) were fitted to measured transition frequencies using Western's program PGOPHER[37] for each molecule,

$$H = H_{\mathrm{R}} - \frac{1}{6}\mathbf{Q}(\mathrm{I}):\nabla\mathbf{E}(\mathrm{I}) \qquad (1)$$

where H_{R} is Watson's A-reduced Hamiltonian[38] in the I^{r} representation for a semi-rigid symmetric top in the case of $H_3N\cdots AgI$. For such symmetric-top species, ground-state rotational constants are denoted by A_0, B_0 and C_0 and the determinable quartic centrifugal distortion constants by D_J and D_{JK} which appear in H_{R}. Fits of the transition frequencies of $H_2O\cdots AgI$, and also of the $D_2HN\cdots AgI$ isotopologue of $H_3N\cdots AgI$, employed the version of H_{R} appropriate to a semi-rigid, nearly-prolate asymmetric top. The only centrifugal distortion constants of $H_2O\cdots AgI$ that contributed significantly to transition frequencies reported here were Δ_J and Δ_{JK}.

The second term of Eqn. (1) describes coupling of the electric quadrupole moment of the I nucleus with the electric field gradient at that nucleus, where $\mathbf{Q}(\mathrm{I})$ is the iodine nuclear quadrupole moment dyadic and $\nabla\mathbf{E}(\mathrm{I})$ is the dyadic of the electric field gradient at the iodine nucleus. The nuclear quadrupole coupling constants of iodine are denoted by $\chi_{aa}(\mathrm{I})$ and $\chi_{bb}(\mathrm{I})-\chi_{cc}(\mathrm{I})$, with the latter required only when fitting the spectra of $H_2O\cdots AgI$. It was unnecessary to include the corresponding term that describes nuclear quadrupole coupling associated with the ^{14}N (I =1) in the Hamiltonian of Eqn. (1) because hyperfine structure arising from this nucleus was not apparent in the observed spectra of $H_3N\cdots AgI$ at the resolution of the present experiments. The naturally-occurring isotopes of silver, ^{107}Ag and ^{109}Ag, each have I = ½ and consequently nuclear electric quadrupole moments of zero. Magnetic nuclear spin-rotation and spin-spin interactions were not observed at the resolution of the present experiments, consistent with previous observations performed on similar molecules. A Kaiser-Bessel window function was used to perform the Fourier transform of data for both $H_3N\cdots AgI$ and $H_2O\cdots AgI$.

The spectroscopic constants evaluated for the various isotopologues of $H_3N\cdots AgI$ and $H_2O\cdots AgI$ are provided in Tables I to IV. Only R-branch, *a*-type transitions[39] having K_{-1} = 0 or 1 were observed for $H_3{}^{14/15}N\cdots{}^{107/109}AgI$, $D_3{}^{14}N\cdots{}^{107/109}AgI$ and $H_2{}^{16/18}O\cdots{}^{107/109}AgI$, as expected for molecules having a large rotational constant A_0, which ensures rotational energy levels having $K_{-1} \geq 2$ are too high in energy to be

detectably populated at the temperature of the expanded gas pulse. The rotational constant, A_0, could not be determined from the available data for either the symmetric-top species, $H_3N\cdots AgI$ or for the nearly prolate asymmetric rotor, $H_2O\cdots AgI$. This parameter was therefore fixed equal to the appropriate calculated values 180 GHz and 60 GHz, when fitting data and simulating spectra for $H_3N\cdots AgI$ and $H_2O\cdots AgI$ respectively. For $H_2{}^{16}O\cdots AgI$ and $H_2{}^{18}O\cdots AgI$, transitions having K_{-1} = 0 or 1 were observed, which allowed determination of (B_0+C_0) and (B_0–C_0). Transitions having K_{-1} = 1 were not observed for $D_2HN\cdots{}^{107/109}AgI$ or $DHO\cdots{}^{107/109}AgI$, so B_0–C_0 was fixed to zero when fitting K_{-1} = 0 transitions for these species. All other isotopologues for which data were recorded are symmetric rotors. The output files of spectroscopic fits performed in PGOPHER are provided as electronic supplementary information.

For the $H_2O\cdots AgI$, $HDO\cdots AgI$ and $H_2{}^{18}O\cdots AgI$ isotopologues, rotational transitions of the type $(J+1) \leftarrow J$ were observed and were regularly separated in energy by a factor of $B_0 + C_0$. As indicated, determination of the $B_0 - C_0$ value for $H_2O\cdots AgI$ and $H_2{}^{18}O\cdots AgI$ was possible due to the detection of $K_{-1} = 1$ transitions. For $HDO\cdots AgI$, only $K_{-1} = 0$ transitions were observed. The ratio of relative intensities of the $K_{-1} = 1$ and $K_{-1} = 0$ transitions (for a given $(J+1) \leftarrow J$) of $H_2O\cdots AgI$ and $H_2{}^{18}O\cdots AgI$ was approximately 3:1 in favour of the former. This strongly implies that $H_2O\cdots AgI$ adopts either a geometry that is planar and of C_{2v} symmetry at equilibrium; or an alternative arrangement that has C_s symmetry at equilibrium, a pyramidal configuration at O, but with a sufficiently low potential energy barrier to the planar C_{2v} form that the wavefunction of the ground vibrational state has C_{2v} symmetry. The orientation of the lone pair on the oxygen atom in the conventional model of the water molecule supports the second of these possibilities, leading to the equilibrium geometry of the general type shown in Figure 3. This conclusion is corroborated by the ab initio calculations at the CCSD(T)(F12)/AVTZ level of theory, which find a barrier to inversion of only 125 cm^{-1}. As a consequence of the described inversion in the vibrational ground state, each of $H_2O\cdots AgI$ and $H_2{}^{18}O\cdots AgI$ contain a pair of protons that are exchanged by a C_2^a rotation and the usual arguments predict a 3:1 nuclear spin statistical weight ratio for $K_{-1} = 1$ to $K_{-1} = 0$ states. Cooling by collisional transfer[40] of population from $K_{-1} = 1$ (triplet) levels to $K_{-1} = 0$ (singlet) levels is a spin forbidden process such that population of the $K_{-1} = 1$ levels remains close to the room temperature value. Consequently, transitions involving levels with $K_{-1} = 1$ are readily observable in our experiment. Conversely, in $HDO\cdots AgI$, the H and D nuclei are not equivalent particles and collisional transfer from $K_{-1} = 1$ to $K_{-1} = 0$ levels is no longer spin-forbidden. Cooling of $K_{-1} = 1$ states then occurs and $K_{-1} = 1$ transitions are not observed.[40] Transitions having $K_{-1} = 1$ are also observed for each of $H_3N\cdots AgI$, consistent with r_0 geometries for each complex that are of C_{3v} symmetry and have $\angle$(N–Ag–I) of 180°. The model geometry of $H_3N\cdots AgI$ is shown in Figure 4. Similar arguments to those presented above explain the absence of $K_{-1} = 1$ transitions for the partially deuterated isotopologues of

$NH_3\cdots AgI$ complex, an observation consistent with previous results obtained through studies of $NH_3\cdots MX$ complexes[12, 13].

C Molecular Geometry

Figures 3 and 4 respectively show the model geometries of the $H_2O\cdots AgI$ and $H_3N\cdots AgI$ complexes. Structural parameters in these models were directly fitted to moments of inertia using Kisiel's STRFIT program[41] to yield r_0 results. For each of the above complexes, isotopic substitutions were available at all atoms except iodine, which permitted measurement of the spectra of six isotopologues of $H_2O\cdots AgI$ and eight isotopologues of $H_3N\cdots AgI$. It was assumed that the r_0 geometries of the isolated H_2O and NH_3 monomers do not change on formation of each complex when determining the remaining r_0 structural parameters. The rationale for the described assumption has been presented previously[10]. Partial substitution structures (r_s) were also determined for $H_2O\cdots AgI$ and $H_3N\cdots AgI$ using Kraitchman's equations[42]. The available isotopic data allows determination of r_s(Ag–O) = 2.232(2) Å for $H_2O\cdots AgI$ (Table V) and r_s(Ag–N) for $H_3N\cdots AgI$ = 2.182(1) Å (Table VI). Under the assumption that the geometry of the NH_3 sub-unit is unchanged from that in the r_0 geometry of H_3N, it is further possible to determine ∠(Ag–N–H) = 110.93(3)° for $H_3N\cdots AgI$. The ab initio calculated geometries of $H_2O\cdots AgI$ and $H_3N\cdots AgI$ are also included in Tables V and VI, respectively. We note that the agreement between the observed and calculated angle ∠Ag···X–H is excellent for X = N but for X = O the experimental value of ϕ is smaller by 4.4 °. The poorer agreement in the case of X = O probably arises because the potential energy barrier to the inversion of configuration at O in $H_2O\cdots AgI$ is low (as it is in $H_2O\cdots AgCl$[10] and $H_2O\cdots AgF$[22]) and therefore this motion makes a large amplitude contribution to the zero-point motion. The ab initio version of the angle is an equilibrium quantity and does not reflect such motion. On the other hand, the inversion is quenched in the case of X = N and there is no corresponding large amplitude contribution to the zero-point motion. We note that the experimental value of ϕ is smaller than its ab initio counterpart in each of $H_2O\cdots AgCl$,[10] $H_2O\cdots CuCl$[10] and $H_2O\cdots AgF$[22]

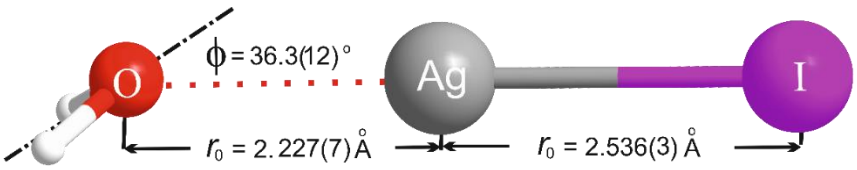

Figure 3 The experimentally determined r_0 geometry of $H_2O\cdots AgI$ drawn to scale (see Table V).

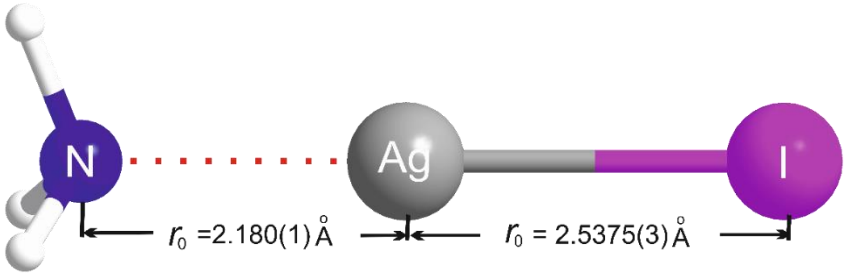

Figure 4. The experimentally determined geometry of $H_3N\cdots AgI$ drawn to scale (see Table VI).

D Intermolecular Stretching Force Constants

We recently proposed a model[43] that allows in principle some of the quadratic force constants of L···M–X complexes to be established from centrifugal distortion constants determined experimentally. This model goes beyond that of Millen[44] by describing the centrifugal distortion constant D_J (for symmetric top or linear complexes) or Δ_J (for asymmetric-top complexes) in terms of three quadratic bond-stretching force constants F_{11}, F_{22} and F_{12}, where the subscripts 1 and 2 respectively refer to the M–X and L···M bonds (such that $F_{11} = F_{M\text{-}X}$ and $F_{22} = F_{L\cdots M}$) with F_{12} being the off-diagonal coupling term. The forms of the equations relating D_J or Δ_J to F_{11}, F_{22} and F_{12} are set out in detail in refs. [7] and [43]. If it is assumed that F_{12} is zero, these equations reduce to eq.(2) when applied to a molecule like $H_2O\cdots AgI$ having effectively C_{2v} symmetry:

$$h\Delta_J = \frac{\hbar^4}{4}\left\{\frac{1}{(I_{bb}^{e})^4} + \frac{1}{(I_{cc}^{e})^4}\right\}\left\{(m_I a_I)^2/F_{11} + \left(m_I\, a_I + m_{Ag}a_{Ag}\right)^2/F_{22}\right\} \qquad (2),$$

where m_{Ag} and m_I are the appropriate nuclide masses, a_{Ag} and a_I are the principal axis coordinates of the Ag and I atoms and $I_{bb}^{e}$and I_{cc}^{e} are the equilibrium principal moments of inertia of the given isotopologue of $H_2O\cdots AgI$. Here it is assumed that zero-point quantities may be used in eq.(2) without serious error. The corresponding form of eq.(2) for D_J of the symmetric-top molecule $H_3N\cdots AgI$ is obtained by setting $I_{bb}^{e} = I_{cc}^{e}$.

By assuming that F_{11} is equal to the force constant of the isolated Ag–I diatomic molecule (145.8 N m^{-1}) [7], F_{22} could be evaluated for $H_2O\cdots AgI$ and $H_3N\cdots AgI$ by fitting the appropriate centrifugal distortion constants. Data for the ^{15}N isotopologues were used in the case of $H_3N\cdots AgI$ because the absence of broadening through unresolved ^{14}N nuclear quadrupole hyperfine structure leads to more accurate values of D_J. The resulting values of F_{22} are compared with the same quantity for several other molecular

complexes of silver iodide in Table VII. Also included in Table VII are the corresponding quantities that arise from the use of the Millen model (these are referred to as k_σ to use Millen's nomenclature). It is clear that the Millen model severely underestimates this force constant, even for cases where the Lewis base is bound relatively weakly to the silver atom, as discussed in refs.7 and 43.

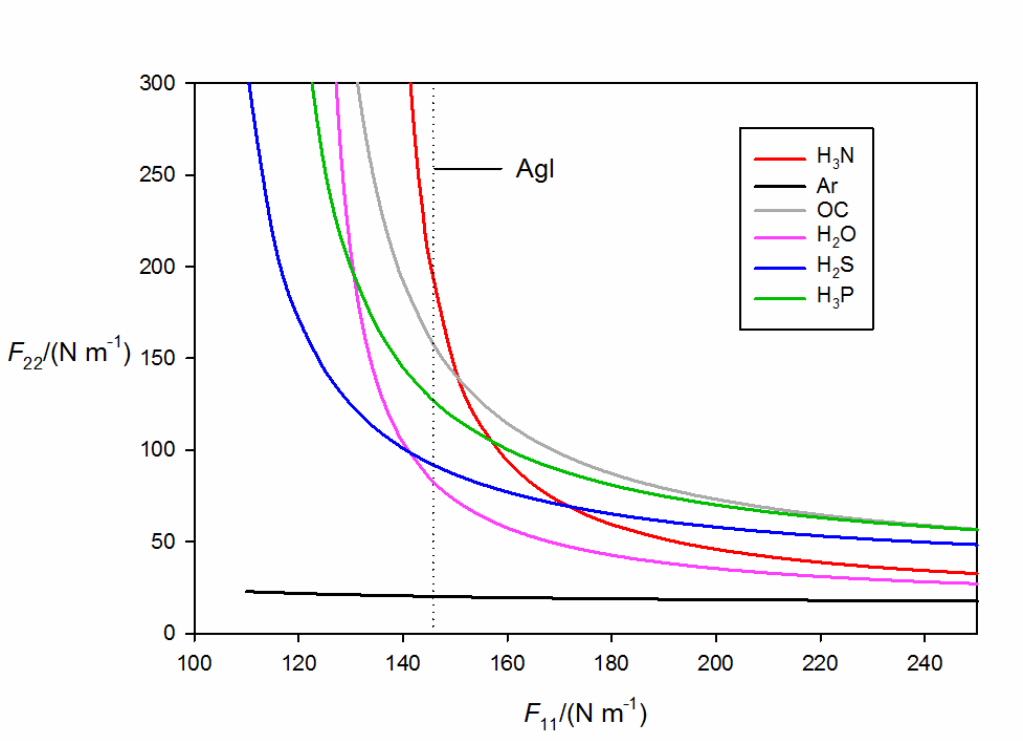

Figure 5. Dependence of F_{22} on the assumed value of F_{11} for various L···AgI complexes. The vertical dotted line indicates the value of the force constant of free AgI.

To inspect the sensitivity of F_{22} to the assumption of unchanged F_{11}, F_{22} was further evaluated over a range of F_{11} values around that of free AgI. A plot showing the variation of F_{22} with the force constant F_{11} is displayed in Figure 5. The horizontal asymptote (where $F_{11} \rightarrow \infty$) represents the case in which AgI can be regarded as rigid, and thus the value then obtained for the force constant F_{22} is equal to that evaluated under the Millen model. The vertical asymptote ($F_{22} \rightarrow \infty$) represents the value of the force constant F_{11} below which a negative, and (therefore unphysical) value of F_{11} is required to fit the centrifugal distortion constant. It is worth noting that the ordering of F_{22} for these complexes is different depending on whether it is assumed that F_{11} is equal to 145.8 N m^{-1} (the value appropriate to the AgI diatomic molecule) or infinity (as would be implicit if L···M–X were approximated as a pseudo-diatomic molecule).. By examining the slope of the curve near F_{11} = 145.8 N m^{-1} it can be seen that the sensitivity of F_{22} to the value of F_{11} changes greatly over the series of Lewis bases shown, with the highest sensitivity being where $F_{11} \approx F_{22}$.

E Electric charge redistribution across the Ag−I bond upon formation of $H_2O\cdots Ag-I$

The ionicity, i_c, or fractional ionic character of the iodine nucleus can be estimated from the expression;

$$i_c = 1 + \frac{\chi_{aa}(\mathrm{I})}{eQq_{(5,1,0)}(\mathrm{I})} \qquad (3)$$

where $eQq_{(5,1,0)}(\mathrm{I})$ is the contribution to the electric field gradient along the *a* inertial axis that arises from a single electron in an iodine $5p_a$ orbital and is equal to 2292.71 MHz[42]. Table VIII compares the ionicities of the complexes studied here with those of other Lewis base-silver iodide complexes similarly obtained. For all these complexes, the ionicity of the Ag−X bond increases upon attachment of the Lewis base. The largest increases are observed for the H_3P, OC and H_2S complexes, all lying between i_c = 0.64 and 0.68, whereas i_c for isolated AgI is 0.537. The complex with H_2O causes a smaller increase in the ionicity of the Ag−X subunit. This is different from the trend observed when these Lewis bases bind to silver chloride [4, 10, 17]. The ordering of the i_c values displayed in Table VIII is also different from the ordering of complexes according to the value of the force constant, F_{22}. It might be expected that the change in charge distribution across the Ag-I bond upon attachment of a Lewis base, as measured by the change in nuclear quadrupole coupling constant, will be approximately proportional to the strength of the interaction of the Lewis base with the silver atom. Whilst this is generally true for the complexes listed in TablesVII and VIII, there are some notable exceptions. The force constant (F_{22}) of the bond formed between water and silver iodide is similar in magnitude to that for the intermolecular bond in $H_2S\cdots AgI$ but the values of i_c for the corresponding complexes span a relatively wide range from 0.61 to 0.66. Likewise NH_3 is calculated to bind more strongly to the silver atom in AgI (F_{22} = 192(38) N m^{-1}) than does H_2S to Ag in $H_2S\cdots AgI$ (F_{22} = 92.0(1.7) N m^{-1}) but has a very similar value of i_c .

IV Conclusions

Two Lewis base - silver iodide complexes, $L\cdots AgI$ (L=H_3N and H_2O), have been generated through laser vaporisation of a solid target in the presence of a gas sample undergoing supersonic expansion and characterized by pure rotational spectroscopy. The basic geometries of complexes studied are qualitatively the same as those established previously for several other members of the $L\cdots AgCl$ series. The values of r(Ag–O) and φ for $H_2O\cdots AgCl$ are 2.229(35) Å and 42(5)° respectively whereas those for $H_2O\cdots AgI$ are 2.227(7) Å and 36.3(12)° respectively. Comparing results for $H_3N\cdots AgCl$ and $H_3N\cdots AgI$, the values of r(Ag–N) are 2.15444(6) Å and 2.180(1) Å respectively. Evidently, the identity of the halogen atom has

only a small effect on structural parameters associated with interactions between L and AgX sub-units. It has previously been noted that φ for $H_2O\cdots AgCl$ is very similar in magnitude to an equivalent parameter in the geometry of $H_2O\cdots HCl$ and $H_2O\cdots CuCl$. These observations are all therefore consistent with a model in which the geometry of each complex is principally determined by the orientation of the lone pair on the oxygen atom which aligns with the axis of the bond in the electrophile acting as the Lewis acid.

Acknowledgements

The authors thank the European Research Council for a postdoctoral fellowship awarded to C.M., a PhD studentship awarded to J.C.M., and for project funding (Grant No. CPFTMW-307000); Newcastle University for PhD studentships awarded to D.M.B. and E.G. The University of Bristol is thanked for a Senior Research Fellowship awarded to A.C.L. S. B. thanks the Ministerio de Educación, Cultura y Deporte of Spain, "Salvador de Madariaga" program, for financial support.

Supplementary Material

See Supplementary Material for the final cycle of the fit to the ground-state rotational spectrum of each reported isotopologue of $H_3N\cdots AgI$ and $H_2O\cdots AgI$ using PGOPHER and the spectroscopic constants thereby determined.

References

1. S. J. Harris, A. C. Legon, N. R. Walker and D. E. Wheatley, Angew. Chem. Int. Ed. **49** (1), 181-183 (2010).
2. G. S. Grubbs II, D. A. Obenchain, H. M. Pickett and S. E. Novick, J. Chem. Phys. **143** (2), 029901 (2015).
3. C. Medcraft, D. M. Bittner, D. P. Tew, N. R. Walker and A. C. Legon, J. Chem. Phys. **145** (19), 194306 (2016).
4. N. R. Walker, D. P. Tew, S. J. Harris, D .E. Wheatley and A. C. Legon, J. Chem. Phys. **135** (1), 014307 (2011).
5. S. Z. Riaz, S. L. Stephens, W. Mizukami, D. P. Tew, N. R. Walker and A. C. Legon, Chem. Phys. Lett. **531**, 1-5 (2012).
6. S. L. Stephens, D. M. Bittner, V. A. Mikhailov, W. Mizukami, D. P. Tew, N. R. Walker and A. C. Legon, Inorg. Chem. **53** (19), 10722-10730 (2014).

7. S. L. Stephens, D. P. Tew, N. R. Walker and A. C. Legon, Phys. Chem. Chem. Phys. **18** (28), 18971-18977 (2016).
8. S. L. Stephens, W. Mizukami, D. P. Tew,. N. R. Walker and A. C. Legon, J. Chem. Phys. **137** (17), 174302 (2012).
9. S. L. Stephens, W. Mizukami, D. P. Tew,. N. R. Walker and A. C. Legon, J. Chem. Phys. **136** (6), 064306 (2012).
10. V. A. Mikhailov,F. J. Roberts, S. L. Stephens, S. J. Harris, D. P. Tew, J. N. Harvey, N. R. Walker and A. C. Legon, J. Chem Phys. **134** (13), 134305 (2011).
11. D. P. Zaleski, S. L. Stephens, D. P. Tew, D. M. Bittner, N. R. Walker and A. C. Legon, Phys. Chem. Chem. Phys. **17** (29), 19230-19237 (2015).
12. D. M. Bittner, D. P. Zaleski. S. L. Stephens,D. P. Tew, N. R. Walker and A. C. Legon, J. Chem. Phys. **142** (14), 144302 (2015).
13. D. M. Bittner, S. L. Stephens, D. P. Zaleski, D. P. Tew, N. R. Walker and A. C. Legon, Phys. Chem. Chem. Phys. **18** (19), 13638-13645 (2016).
14. C. J. Evans, L. M. Reynard and M. C. L. Gerry, Inorg. Chem. **40** (24), 6123-6131 (2001).
15. G. S. Grubbs ii,, D. A. Obenchain,. H. M. Pickett and S. E. Novick, J Chem. Phys.**141** (11), 114306 (2014).
16. D. A. Obenchain,, D. S. Frank, G. S. Grubbs II, H. M. Pickett and S. E. Novick, J. Chem. Phys. **146** (20), 204302 (2017).
17. C. Medcraft, J. C. Mullaney, N. R. Walker and A. C. Legon, J. Mol. Spectrosc. **335**, 61-67 (2017).
18. C. J. Evans, A. Lesarri and M. C. L. Gerry, J. Amer. Chem. Soc. **122** (25), 6100-6105 (2000).
19. C. J. Evans and M. C. L. Gerry, J. Chem. Phys. **112** (3), 1321-1329 (2000).
20. L. M. Reynard, C. J. Evans and M. C. L. Gerry, J. Mol. Spectrosc. **206** (1), 33-40 (2001).
21. S. A. Cooke and M. C. L. Gerry, Phys. Chem. Chem. Phys. **6** (13), 3248-3256 (2004).
22. S. L. Stephens, D. P. Tew, N. R. Walker and A. C. Legon, J. Mol. Spectrosc. **267** (1–2), 163-168 (2011).
23. S. L. Stephens and N. R. Walker, J. Mol. Spectrosc. **263** (1), 27-33 (2010).
24., D. Loru, M. A. Bermúdez and M. E. Sanz, J. Chem. Phys. **145** (7), 074311 (2016).
25. H.-J. Werner, P. J. Knowles, G. Knizia, F. R. Manby and M. Schütz, Wiley Interdisciplinary Reviews: Computational Molecular Science **2** (2), 242-253 (2012).
26. TURBOMOLE V7.1, a Development of the University of Karlsruhe, 1989-2007 and TURBOMOLE GmbH, since 2007, available at http./www.turbomole.com
27. C. Hättig, D. P. Tew and A. Köhn, J. Chem. Phys. **132** (23), 231102 (2010).
28. C. Hättig, W. Klopper, A. Köhn and D. P. Tew, Chem. Rev. **112** (1), 4-74 (2012).

29. K. Raghavachari, G. W. Trucks, J. A. Pople and M. Head-Gordon, Chem. Phys. Lett. **157** (6), 479-483 (1989).
30. K. A. Peterson, D. Figgen, E. Goll, H. Stoll and M. Doig, J. Chem. Phys. **119** (21), 11113-11123 (2003).
31. I. S. Lim, P. Schwerdtfeger, B. Metz and H. Soll,, J. Chem. Phys. **122** (10), 104103 (2005).
32. A. Hellweg, C. Hättig, S. Höfener and W. Klopper, Theo. Chem. Accounts **117** (4), 587-597 (2007).
33. E. F. Valeev, Chem. Phys. Lett. **395** (4), 190-195 (2004).
34. S. L. Stephens, N. R. Walker and A. C. Legon, Phys.Chem. Chem. Phys. **13** (46), 20736-20744 (2011).
35. S. G. Batten, A. G. Ward and A. C. Legon, J. Mol. Struct. **780–781**, 300-305 (2006).
36. R. D. Thomas and J. S. Muenter, J. Chem. Phys. **60** (7), 2929-2930 (1974).
37. C. M. Western, J. Quant. Spectrosc. and Rad. Trans. **186**, 221-242 (2017).
38. J. K. G. Watson,, J. Chem. Phys. **46** (5), 1935-1949 (1967).
39. S. A. Cooke and P. Ohring, Journal of Spectroscopy, Vol.2013, 1-10 (2013). http://dx.doi.org/10.1155/2013/698392
40. E. Knozinger, P. Suppan and A. C. Legon, Faraday Discuss. Chem. Soc. **86**, 269-270 (1988).
41. Z. Kisiel, J. Mol. Spectrosc. **218**, 58-67 (2003).
42. R. L. Cook and Walter Gordy, *Microwave Molecular Spectra*, 1st ed. (Interscience Publishers, Durham, North Carolina, 1970).
43. D. M. Bittner. N. R. Walker and A. C. Legon, J. Chem. Phys. **144** (7), 074308 (2016).
44. D. J. Millen, Can. J. Chem. **63** (7), 1477-1479 (1985).

Tables

TABLE I. Experimentally-determined spectroscopic constants of isotopologues of $H_3N\cdots AgI$.

	$H_3N\cdots{}^{107}AgI$	$H_3N\cdots{}^{109}AgI$	$D_3N\cdots{}^{107}AgI$	$D_3N\cdots{}^{109}AgI$
B_0 / MHz	866.07484(54)	862.33436(78)	808.39412(51)	805.38125(72)
D_J / kHz	0.0867(33)	0.0817(44)	0.0628(22)	0.0602(32)
D_{JK} / kHz	8.65(30)	8.46(27)	7.00(24)	6.97(15)
χ_{aa}(I) / MHz	−795.42(54)	−795.31(69)	−794.61(72)	−793.40(76)
N[b]	18	24	19	19
$\sigma_{r.m.s.}$[c] / kHz	9.9	11.3	10.0	6.9

[a] Numbers in parentheses are the standard deviation in units of the last significant figure.
[b] Number of nuclear quadrupole hyperfine components included in the fit.
[c] Root mean square deviation of the fit.

TABLE II. Experimentally-determined spectroscopic constants of isotopologues of $H_3N\cdots AgI$ containing ^{15}N or D.

	$H_3{}^{15}N\cdots{}^{107}AgI$	$H_3{}^{15}N\cdots{}^{109}AgI$	$D_2HN\cdots{}^{107}AgI$	$D_2HN\cdots{}^{109}AgI$
$(B_0+C_0)/2$ / MHz	850.20711(23)[a,b]	846.68607(30)[b]	1653.1886(38)	1646.7204(34)
D_J / kHz	0.0645(12)	0.0662(14)	[0.0628][c]	0.0611(75)[c]
D_{JK} / kHz	8.62(13)	8.55(17)	-	-
χ_{aa}(I) / MHz	−796.90(26)	−796.60(31)	−794.3(19)	−795.9(30)
N[d]	41	28	6	11
$\sigma_{r.m.s.}$[e] / kHz	7.3	8.1	9.7	14.0

[a] Numbers in parentheses are the standard deviation in units of the last significant figure.
[b] Results for $H_3{}^{15}N\cdots{}^{107}AgI$ and $H_3{}^{15}N\cdots{}^{109}AgI$ are included in this table for concise presentation. Note that $B_0 = C_0 = (B_0+C_0)/2$ for this symmetric rotor.
[c] Watson's *A* reduction was employed.
[d] Number of nuclear quadrupole hyperfine components included in the fit.
[e] Root mean square deviation of the fit.

TABLE III. Experimentally determined spectroscopic constants of isotopologues of $H_2O\cdots AgI$.

	$H_2O\cdots{}^{107}Ag^{127}I$	$H_2O\cdots{}^{109}Ag^{127}I$	$H_2{}^{18}O\cdots{}^{107}Ag^{127}I$	$H_2{}^{18}O\cdots{}^{109}Ag^{127}I$
(B_0+C_0) / MHz	1690.1972(28)[a]	1683.2961(28)	1629.6036(72)	1623.486(13)
(B_0-C_0) / MHz	1.64674(20)	1.63346(20)	1.52831(40)	1.51669(46)
Δ_J / kHz	0.07072(79)	0.07111(77)	0.0649(17)	0.0593(28)
Δ_{JK} / kHz	8.642(91)	8.626(87)	8.80(17)	8.69(19)
χ_{aa}(I) / MHz	–885.54(11)	–885.33(10)	–884.24(49)	–885.10(71)
$(\chi_{bb}(I)-\chi_{cc})$(I) / MHz	–12.73(28)	–12.79(25)	–13.6(13)	–13.2(17)
N[b]	75	68	40	27
$\sigma_{r.m.s.}$[c] / kHz	5.5	5.1	9.6	9.3

[a] Numbers in parentheses are the standard deviation in units of the last significant figures.
[b] Number of nuclear quadrupole hyperfine components included in the fit.
[c] Root mean square deviation of the fit.

TABLE IV. Experimentally determined spectroscopic constants of isotopologues of HDO···AgI.

	HDO···^{107}Ag^{127}I	HDO··· ^{109}Ag^{127}I
(B_0+C_0) / MHz	1648.9189(38)[a]	1642.5292(60)
Δ_J / kHz	0.0679(10)	0.07090(16)
χ_{aa}(I) / MHz	–885.08(24)	–884.42(41)
$(\chi_{bb}(\mathrm{I})-\chi_{cc}(\mathrm{I}))$ / MHz	-	-
N[b]	28	26
$\sigma_{r.m.s.}$[c] / kHz	5.3	7.5

[a] Numbers in parentheses are the standard deviation in units of the last significant figures.
[b] Number of nuclear quadrupole hyperfine components included in the fit.
[c] Root mean square deviation of the fit.

TABLE V. r_0 and r_e geometries of H_2O···AgI.

	Exptl. (r_0)	Calc. (r_e)[a]
r(Ag–I)/Å	2.536(3)	2.5374
r(Ag–O)/Å	2.227(7)[b]	2.2329
r(H–O)/Å	[0.95785]	0.9605
φ / °	36.3(12)	40.74

[a] Calculated *ab initio* at the CCSD(T)(F12*)/AVTZ level.
[b] The coordinates determined for the silver and oxygen atoms imply a r_s result of 2.232(2) Å for this parameter.

TABLE VI. r_0, r_s and r_e geometries of H_3N···AgI.

	Exptl. (r_0)	Exptl. (r_s)	Calc. (r_e)[a]
r(Ag–I)/Å	2.5375(3)	-	2.5457
r(Ag–N)/Å	2.180(1)	2.182(1)	2.1767
r(H–N)/Å	[1.01699]	[1.01619]	1.0128
∠(Ag–N–H) /°	110.86(5)	110.93(3)	111.64

[a] Calculated *ab initio* at the CCSD(T)(F12*)/AVQZ level.

TABLE VII. Experimentally-determined quadratic force constants, F_{22}, for L···AgI complexes (L= Ar, H_3N, H_2O, H_2S, H_3P or CO).

	F_{22} (N m^{-1})[a]	k_σ (N m^{-1})[b]
Ar···AgI[c]	20.2(8)	14.8
H_2O···AgI[d]	83(3)	13.9
H_2S···AgI[e]	92.0(17)	29.0
H_3P···AgI[f]	122(5)	31.7
OC···AgI[g]	156(26)	47
H_3N···AgI[d]	192(38)	15.1

[a]Calculated by using the two-force constant model to fit D_J values, assuming F_{11} = 145.8 N m^{-1}, the value for free AgI in its vibrational ground state. Numbers in parentheses are one standard deviation of the fit in units of the last significant figures

[b]k_σ values were determined from D_J values by means of the model described by Millen (ref.44).

[c]Ref. 17

[d] This work.

[e] Ref. 3

[f] Ref. 7

[g] Ref. 9. F_{22} recalculated from D_J values reported in this reference.

TABLE VIII. Ionicity of Ag–I in complexes L···AgI complexes (where L= Ar, H_3N, H_2O, H_2S, H_3P or CO).

Molecule	χ_{aa}(I)	i_c [a]
Ag-I	-1062.5299(15)[b]	0.537
Ar···AgI[c]	−985.411(54)	0.570
H_2O···AgI	-885.54(11)	0.613
H_2S···AgI[d]	-807.36(4)	0.648
H_3N···AgI	-795.42(54)	0.65
OC···AgI[e]	−769.84(22)	0.66
H_3P···AgI[f]	-733.83(34)	0.68

[a] Calculated using Eq. (2) and $eQq_{(5,1,0)}(I)$ values cited in Ref. 43

[b] Ref. 35

[c] Ref. 17

[d] Ref. 3

[e] Ref. 9

[f] Ref. 7